Photochemical CO_2 reduction in water using a co-immobilised nickel catalyst and a visible light sensitizer

*Gaia Neri,[a,b] Mark Forster,[a,b] James J. Walsh,[a,b] C. M. Robertson,[a] T. J. Whittles,[b,c] Pau Farràs[d] and Alexander J. Cowan[a,b]**

Electronic supporting information

Contents

1. Experimental:

The starting materials and solvents for synthesis were purchased from Sigma Aldrich, Fisher Scientific or VWR, and were used without further purification. ZrO_2 was

purchased from Sigma (nanopowder, >100 nm, 25 m^2 g^{-1}). ZrO_2 films (20 - 30 nm) were prepared from colloidal pastes doctor bladed onto TEC-15 glass (Pilkington) in the manner previously described.[1] Milli-Q water (18.2 MΩ) was used throughout. Ar, N_2 and CO_2 were purchased from BOC at CP or higher grade. The pH of aqueous electrochemistry solutions were adjusted by adding 1 M $HClO_4$ or NaOH to the pre-purged solution until the desired value was reached, measuring with a Hannah pH probe, which was calibrated daily. Sodium ascorbate and ascorbic acid (≥ 99% purity) solutions were prepared freshly for each experiment. RuP was prepared as previously described.[2]

1.1 Synthesis of [Ni(CycP)]n - [Ni([(1,4,8,11-tetraazacyclotetradecan-1-yl)methylene]phosphonic acid)]n*:* [1,4,8,11-tetraazacyclotetradecan-1-yl)methyl]phosphonic acid (CycP) was prepared in the manner previously reported.[3] In a 50 ml round-bottomed flask equipped with a magnetic stirring bar CycP (630 mg, 1.1 eq.) was dissolved in water. Sodium bicarbonate (850 mg, 5.5 eq.) was added. Gas was evolved. $NiCl_2 \cdot 6H_2O$ (440 mg, 1 eq.) was added. The solution changed colour from green to purple within the first 15 minutes and became cloudy after 30 minutes. The mixture was left stirring at room temperature for three hours. The precipitate was filtered off, and the solvent rotary evaporated to dryness. The remaining lilac powder was dissolved in methanol, the undissolved solid was filtered off and the solvent was evaporated. The product was then purified by loading the crude on a silica gel column and eluting with a MeOH:NH_3 9:1 mixture as the mobile phase. Lilac crystalline powder; obtained: 267 mg, yield = 35%; $C_{11}H_{25}N_4NiO_3P \cdot 0.3H_2O$ (350.1): calcd. N 15.72, H 7.24, C 37.07; found N 15.46, H 7.46, C 37.32; ***m/z*** (**ESI):** 351.1 $(M+H)^+$; 373.1 $(M+Na)^+$; ATR-FTIR (v, cm^{-1}): 3384 (br.), 3146 (br.), 2914, 2840, 1651, 1459, 1454, 1436, 1102 (st.), 1055 (v.st.), 967 (st.), 874.

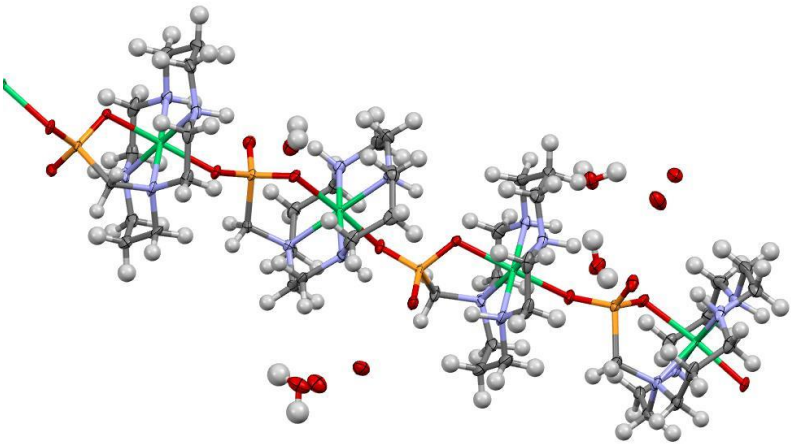

Figure S1 – ORTEP diagram of the crystal structure of [Ni(CycP)]n

Single crystals of Ni(CycP) were grown from slow evaporation of water. A suitable crystal was mounted on a MiTeGen tip using mounting oil and the data were measured at 100 K using Mo wavelengths on a Bruker Venture D8 diffractometer fitted with a Photon 100 detector. The software package *APEX3*[4] was used for data collection, integration and scaling; *OLEX2*[5], along with the *SHELX*[6] suite of programs were used for structural solution and refinement. The crystals selected for the experiment were visually representative of the batch, as confirmed by rigorous sample screening. Upon close inspection with X-ray radiation, all crystals appeared twinned. However no satisfactory twin law was found that yielded a stable refinement when employed.

NiCycP crystallises in a polymeric structure $[Ni(CycP)]_n$ with supporting lattice waters (confirmed by elemental analysis); the chains propagate diagonally along the *c*-axis. The lattice waters, of which some hydrogen positions could not be satisfactorily modelled, form a hydrogen bonding network which link neighbouring chains together. The chains appear to form a pseudo closed packed structure, as is consistent with many linear polymeric materials.

1.2 Catalyst immobilisation

General procedure for the preparation of ZrO_2/RuP/NiCycP nanoparticles: ZrO_2 either in a powder or film form was calcined at 350°C for 30 minutes prior to RuP/NiCycP immobilisation. RuP and NiCycP were immobilised from ethanolic solutions with NiCycP at 0.1 mM unless otherwise specified. The concentration of RuP was adjusted to obtain the desired ratio of catalyst and dye, see Table S1. For RuP only samples 0.5 mM RuP ethanolic solutions were employed. 10 mg of ZrO_2 was used per ml of ethanolic solution and samples were stirred for 48 hours at room temperature before being centrifuged (3x30 mins at 8000 RPM) and washed with ethanol. Prior to photocatalysis experiments being carried out particles were dried under vacuum and stored in the dark. ZrO_2/RuP and ZrO_2/RuP/NiCycP films (*ca.* 1 cm^2) were soaked in 5 ml of ethanolic solution of the desired [RuP]:[NiCycP] for 48 hours then rinsed with copious quantities of ethanol before being dried under a stream of compressed air and under vacuum for 2 hours.

ZrO_2/Ru/NiCycP samples were studied by FTIR-ATR spectroscopy (Pike accessory on a Bruker Vertex), UV/Vis spectroscopy (Shimadzu 2300) and XPS. XPS measurements were performed in a standard ultrahigh vacuum (UHV) chamber operating at a base pressure of less than 2×10^{-10} mbar with hydrogen as the main residual gas, using a PSP Vacuum Technology non-monochromatic Al K_α X-ray source (hv = 1486.6 eV) typically operating at 144 W, together with a PSP Vacuum Technology electron-energy analyzer operating with a typical constant pass energy of 20 eV. Calibration of the spectrometer was performed using a polycrystalline silver foil, cleaned *in vacuo*. The Ag $3d_{5/2}$ photoelectron line had a binding energy (BE) of 368.3 eV and a full-width at half-maximum (FWHM) of 1.2 eV. Charge compensation was achieved by setting the binding energy of the main adventitious C 1s peak to 285.0 eV.

1.3 Electrochemical studies: All electrochemical experiments were carried out using a Palmsens[3] potentiostat (Alvatek). Electrochemical measurements of NiCyc and NiCycP in solution were carried out using a 4-neck pear-shaped flask with a platinum basket counter electrode, Ag/AgCl (3.5 M NaCl, IJ Cambria) reference electrode and a hanging mercury drop working electrode (WK2) using triply distilled mercury (Fisher). The surface area of a mercury drop was typically 0.023 cm^2. Electrochemical measurements on ZrO_2 films were carried out in a custom-built four-necked cell, using

a platinum wire counter electrode, a ZrO_2 or ZrO_2/NiCycP film as the working electrode and a silver wire *quasi* reference electrode. The Ag wire was referenced to the ferrocene redox couple using an additional glassy carbon working electrode.

1.4 Photocatalytic studies: In a typical experiment 2 mg of ZrO_2/RuP/NiCycP nanoparticles were suspended in 2 ml of freshly prepared ascorbate buffer 0.1 M (pH 4) in a 5 ml glass vial equipped with a magnetic stirring bar and a septum screw cap. The vial was sealed and purged with either argon or CO_2 for 30 minutes. The sample was illuminated with either a 150 W Xe arc lamp (Applied Photophysics) or a 300 W Xe lamp (LOT Quantum Design) under constant stirring. The IR radiation was filtered with a KG1 filter (Thorlabs), and experiments also used either a 375 or 420 nm long pass filters (Thorlabs or Edmund Optics). The light intensity incident on the glass vial was measured with an optical power meter and a thermal sensor (Thorlabs). Experiments were carried out either at 50 mW cm^{-2} (Figure S11, Figure S13, Figure S14) or 40 mW cm^{-2} (all other experiments). Care was taken to ensure that the entirety of the sample was illuminated during experiments. The nature of the reaction products were verified by gas chromatography using an Agilent 6890N instrument with helium N6 (BOC) as the carrier gas (5 mol min^{-1}), equipped with a 5 Å molecular sieve column (ValcoPLOT, 30 m length, 0.53 mm ID) and a pulsed discharge detector (D-3-I-HP, Valco Vici). The peak areas for H_2 and CO were quantified by calibration with a custom-ordered calibrant gas containing 500 ppm of H_2 and 200 ppm of methane and CO (Calgaz). Calibrations were carried out daily. NMR spectroscopy of post-reaction solutions did not show the presence of any liquid based CO_2 reduction products at detectable concentrations.

1.5 Transient and steady state spectroscopy: Transient UV/Vis spectra were recorded using apparatus that has been previously described.[7] Briefly, argon or CO_2 purged samples placed in quartz cuvettes and excited at 355 nm (150 μJ cm^{-2}, 0.33 H_z, 6 ns pulse width) by the third harmonic of a Nd:YAG laser (Continuum Surelite). Changes in optical density were measured using a 75 W Xe lamp (OBB, powerarc), monochromators (OBB) both pre and post sample and a Si photodiode (Hamamatsu S3071). The photodiode output was coupled to a home-made amplifier to provide a system with an approximate time resolution of ~2 μs. Typically 300 individual laser shots are averaged at each wavelength. Transient spectra of ZrO_2 based samples were recorded using ZrO_2 films due to the high level of scattering from the ZrO_2

suspensions used in photocatalytic studies. RuP* emission from ZrO_2/RuP films was measured using both steady state (Perkin-Elmer LS55) and time-resolved approaches. Samples were studied either in 0.1 M ascorbate buffer (pH 4) or in water at pH 4 (HCl) purged with Ar. In the time resolved experiments samples were excited by a UV laser (355 nm, 6 ns, <40 $\mu J\ cm^{-2}$, 0.5 H_z) and the RuP* emission at 650 nm was passed through a monochromator (OBB) and a long pass 400 nm filter (OD 4, Edmund optics) before detection by a fast Si photodiode (HCA-S-200M) coupled to an amplifier (HVA-200M-40-B). The instrument response function of the system was measured from the scattered 355 nm light off a $BaSO_4$ sample, with the 400 nm long pass filter removed and found to be on the order of 10 ns at the gain levels and oscilloscope settings used. Kinetic traces were recorded by averaging 128 laser shots.

2. Supporting experiments:

2.1. ICP analysis:

5 mg samples of ZrO_2/RuP/NiCycP were soaked thoroughly in 5 ml of NaOH (1 M) for 12 hours to desorb both the RuP and NiCycP. The resultant solution was centrifuged prior to analysis by ICP-OES (SPECTRO CIROS with axial mode of detection). The concentrations in brackets in the first column indicate those of the individual components in the original ethanolic solution used to sensitize the ZrO_2 nanoparticles. Table S1 gives the values for the samples used in figure S11. To calculate photocatalytic rates normalised for the mass of RuP+NiCycP ICP measurements were carried out on every batch of nanoparticles prepared. ICP analysis confirmed the presence of both Ru and Ni on the ZrO_2/RuP/NiCycP samples. Notably, post-photocatalysis we observed no significant Ni or Ru (<5%) leaching into the experiment

solution, indicating the stability of the ZrO_2/RuP/NiCycP samples.

Sample ([RuP]:[NiCycP])	ICP concentration (nmol mg^{-1})		Achieved molar ratio on ZrO_2 (RuP:NiCycP)
	Ru	Ni	
1:1 ([1 x 10^{-4} M]:[1 x 10^{-4} M])	2.84	5	0.6
2.5:1 ([2.5 x 10^{-4} M]:[1x 10^{-4} M])	6.55	2.70	2.4
5:1 ([5 x 10^{-4} M]:[1 x 10^{-4} M])	8.90	3.40	2.6
10:1 ([1 x 10^{-3} M]:[1 x 10^{-4} M])	10.40	0.72	14.4
RuP alone	5.14	-	-
Post experiment solution (5:1)	0.6	-	-

Table S1 - ICP analysis of ZrO_2/RuP/NiCycP samples

2.2. UV/Vis spectroscopy:

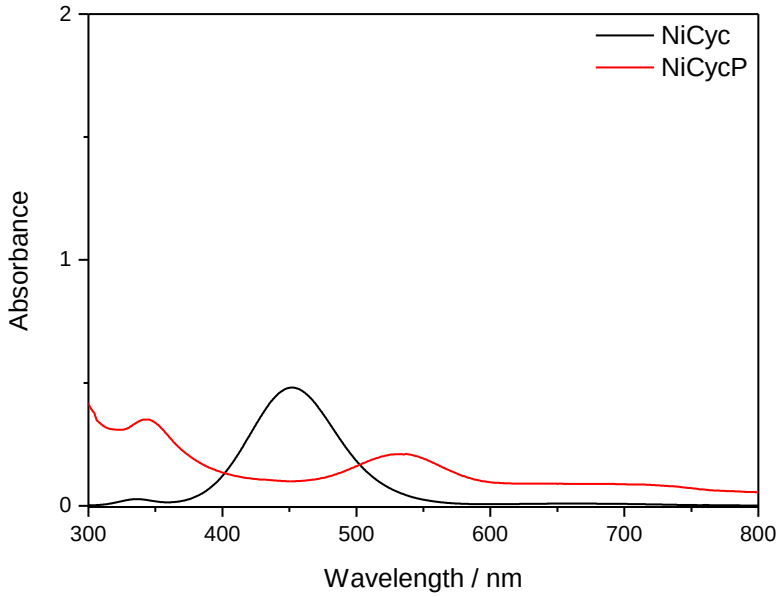

Figure S2 - Solution UV-Vis spectra of NiCyc and NiCycP (10 mM in water, 1 cm pathlength).

The behaviour of NiCycP is distinct from NiCyc in aqueous solution. While the latter exists in an equilibrium of square planar and octahedral coordination geometries, with the square planar being the most abundant especially in non-coordinating solvents, NiCycP forms solutions with a UV-vis spectrum (Figure S2) characterised by two

absorption peaks, at 344 nm (ε = 24 $M^{-1}cm^{-1}$) and at 533 nm (ε = 12 $M^{-1}cm^{-1}$), suggesting an octahedral structure is the dominant form, in line with the crystal structure. [8]

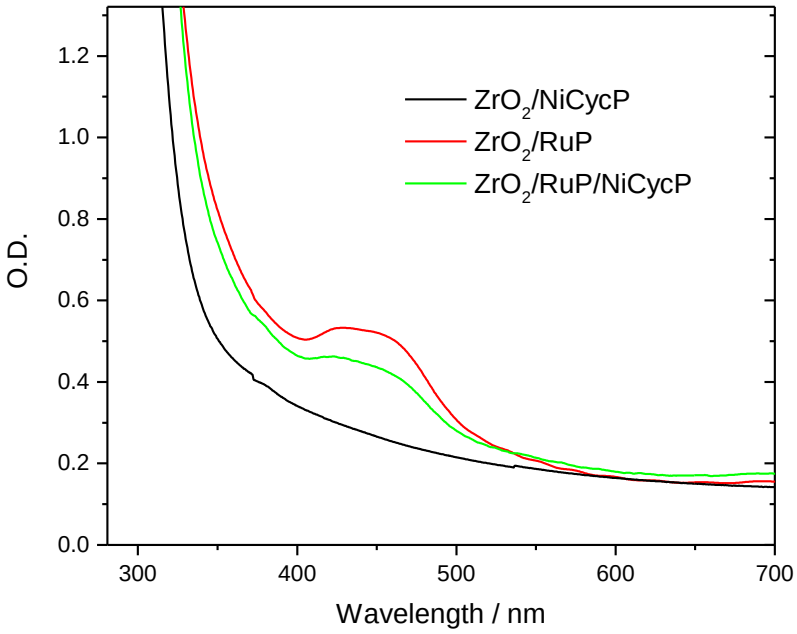

Figure S3 - UV/Vis spectra of ZrO_2/NiCycP, ZrO_2/RuP and ZrO_2/RuP/NiCycP films.

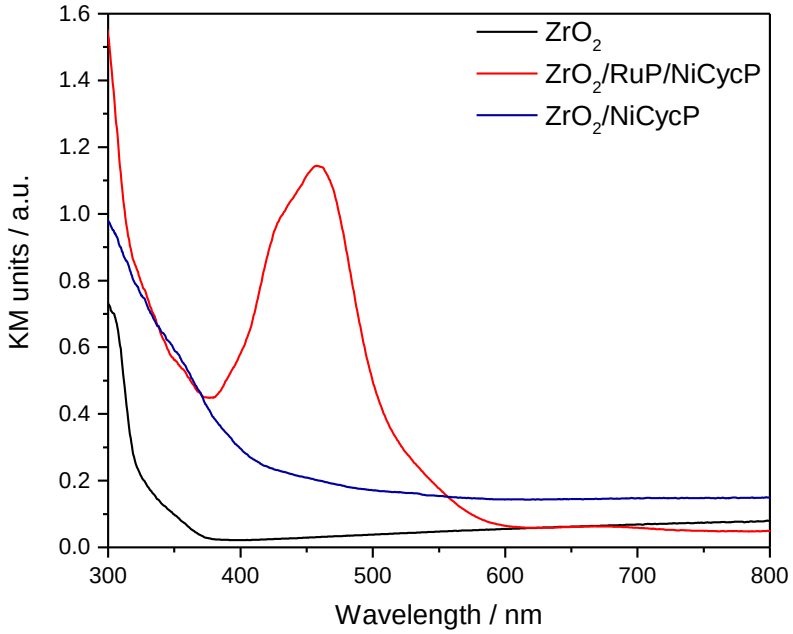

Figure S4 - DR UV/Vis spectra of ZrO_2/RuP/NiCycP powders used in the photocatalysis studies, transformed using the Kubelka-Munk function

Immobilised RuP ($\varepsilon_{458\ nm}$ = 9300 $M^{-1}cm^{-1}$, solution[2]) is readily observable on the ZrO_2 samples (both films and powder) with a spectrum that is in good agreement with previous literature studies,[9] confirming that RuP has been successfully immobilised on the ZrO_2 support. The spectrum of ZrO_2 powder modified with NiCycP only shows very weak shoulder bands at 452 and 351 nm compared with the spectrum of unmodified ZrO_2, this is tentatively assigned to the presence of the bound NiCycP. The shoulder at 452 nm, typical of square-planar macrocyclic complexes of nickel, indicates that the phosphonate group is uncoordinated for a part of the bound complex, in agreement with the FTIR spectra below. However UV/Vis spectroscopy of NiCycP on a ZrO_2 film did not show any discernible features beyond those of ZrO_2, this is due to the low extinction coefficient of NiCycP (in solution octahedral NiCycP $\varepsilon_{533\ nm}$ = 12 $M^{-1}cm^{-1}$) in the visible region.

2.3. FTIR spectroscopy:

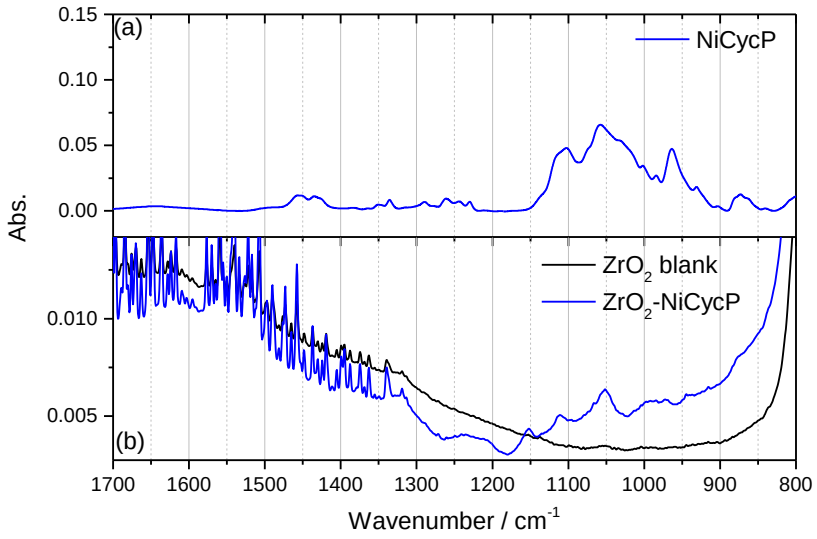

Figure S5 - ATR-FTIR spectrum of NiCycP (a) and spectrum of ZrO_2 particles following soaking in an ethanolic NiCycP solution.

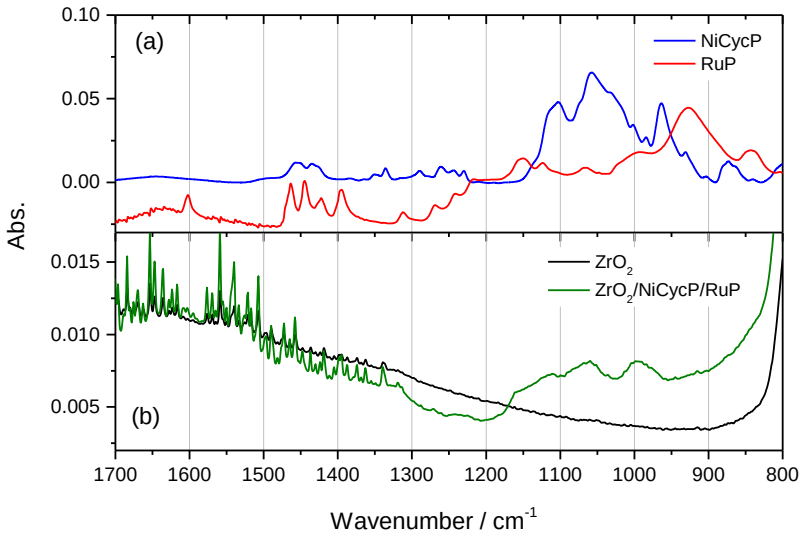

Figure S6 - ATR-FTIR spectra of NiCycP (blue) and RuP (red) (a) and spectrum of ZrO_2 particles following soaking in an ethanolic NiCycP/RuP solution (green).

The ATR-FTIR spectrum of NiCycP (Figure S5(a)) has distinctive bands at 1103 and 1031 cm^{-1} assigned to the ν_{as}(PO) and ν_s(PO) modes, respectively, with a further band at 1057 cm^{-1} assigned to a $\nu_{as}(PO_3)$ mode.[10–12] The absence of a broad peak between 1200 and 1150 cm^{-1}, typical of P-O-H bonds, is in agreement with the crystal structure of solid NiCycP that has a polymer structure with each phosphonate group coordinating to an adjacent Ni centre. Untreated ZrO_2 has a broad featureless IR spectrum at > 900 cm^{-1}. Following soaking in an ethanolic solution of NiCycP, and washing with ethanol to remove any unbound NiCycP we observe the presence of IR bands assigned to the Ni complex bound to ZrO_2, demonstrating that the surface immobilisation approach has been successful, Figure S5. It is notable that the sharp peak at 963 cm^{-1} assigned to a Ni-O-P mode[12] observed for NiCycP is absent in the spectrum of ZrO_2/NiCycP and that a new IR band at 1152 cm^{-1}, tentatively assigned to a P-O-H mode is present. Immobilisation of both RuP and NiCycP on ZrO_2 leads to a complex overlapped IR spectrum in the 1300-900 cm^{-1} region, Figure S6. The binding of RuP to ZrO_2 has been studied elsewhere[1] in multiple reports and it is found that UV/Vis is a more useful technique to monitor the immobilisation of RuP in the presence of NiCycP on ZrO_2, see section S2.2

2.4. XPS:

The presence of the RuP complex on ZrO_2 was also further verified by analysing the Ru 3d peaks; these are heavily overlapped with the C 1s peaks, however the small concentration of complex on the surface prevents identification of other ruthenium peaks, which will have lower intensity. The binding energy of the Ru $3d_{5/2}$ peak is in agreement with past reports for a Ru^{2+} oxidation state Figure S7.[13–15] Following photocatalysis XPS indicated no shift in the binding energy of the Ru $3d_{5/2}$ peak. However it is notable that during the XPS measurement the Ru peak is seen to decrease in intensity with time indicating that the RuP is unstable during prolonged XPS measurements (Figure S8). Therefore the binding energies of the molecular species must be interpreted with caution. An approximate measure of the intensity of the Ru $3d_{5/2}$ peak pre- and post-catalysis was obtained from a rapid initial low resolution survey scan, which indicated minimal loss of Ru, in-line with the ICP analysis above, Figure S9. For the optimal ZrO_2/NiCycP/RuP samples used in the catalysis studies the nickel peaks are very small due the low loading of Ni (see section 2.1), preventing meaningful interpretation of XPS spectrum pre- and post-catalysis. Therefore we studied a ZrO_2/NiP sample in the absence of RuP to explore the immobilisation of NiCycP, Figure S10. The strongest signal is given by the Ni $2p_{3/2}$ peak In agreement with past reports[16,17] the nickel oxidation state in ZrO_2/NiCycP is assigned to Ni^{2+} and we see a good agreement with the XPS spectrum of the unbound catalyst.

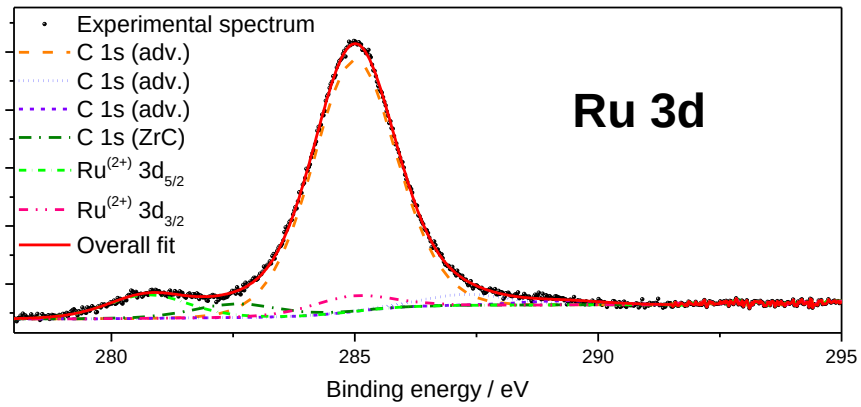

Figure S7 - Experimental and simulated XPS spectra of Ru 3d levels for ZrO2/NiCycP/RuP sample

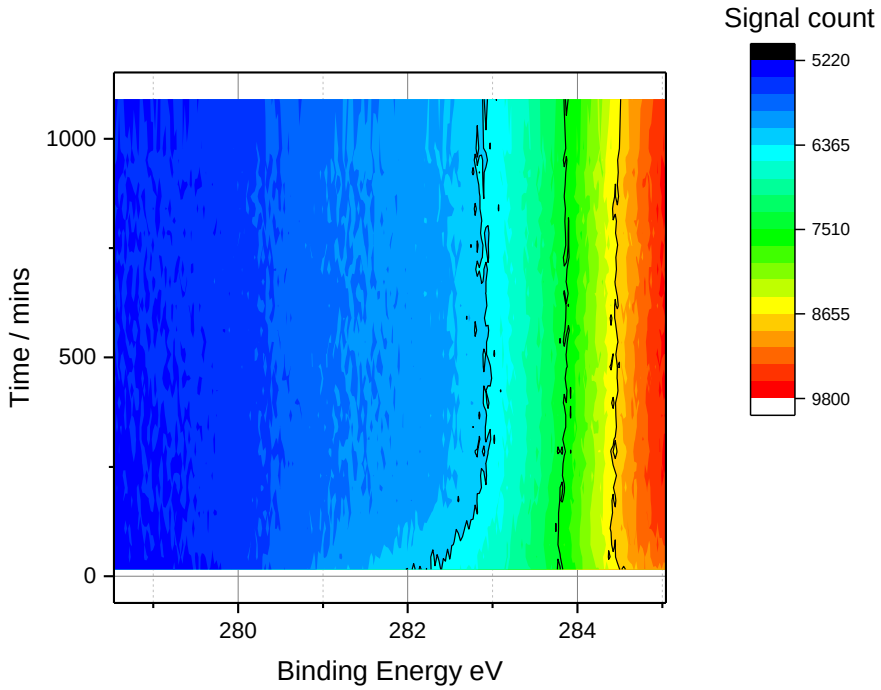

Figure S8 - Experimental XPS spectra showing the loss of the shoulder assigned to the Ru $3d_{5/2}$ peak during the XPS measurement.

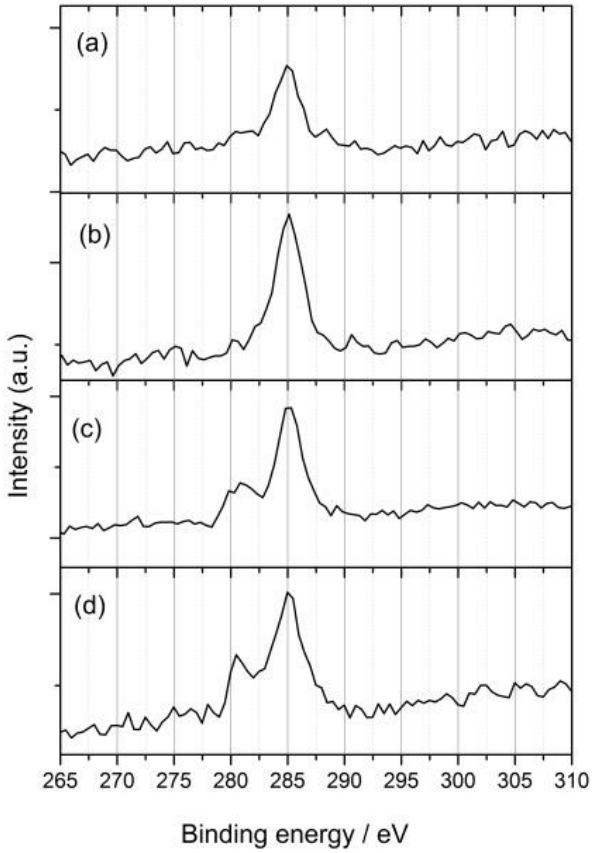

Figure S9 - Low resolution XPS spectra of Ru 3d region for (a) ZrO_2, (b) ZrO_2/NiCycP, (c) ZrO_2/NiCycP/RuP, (d) and ZrO_2/NiCycP/RuP post catalysis showing the presence of the Ru^{2+} in the post catalysis (48 hr) sample.

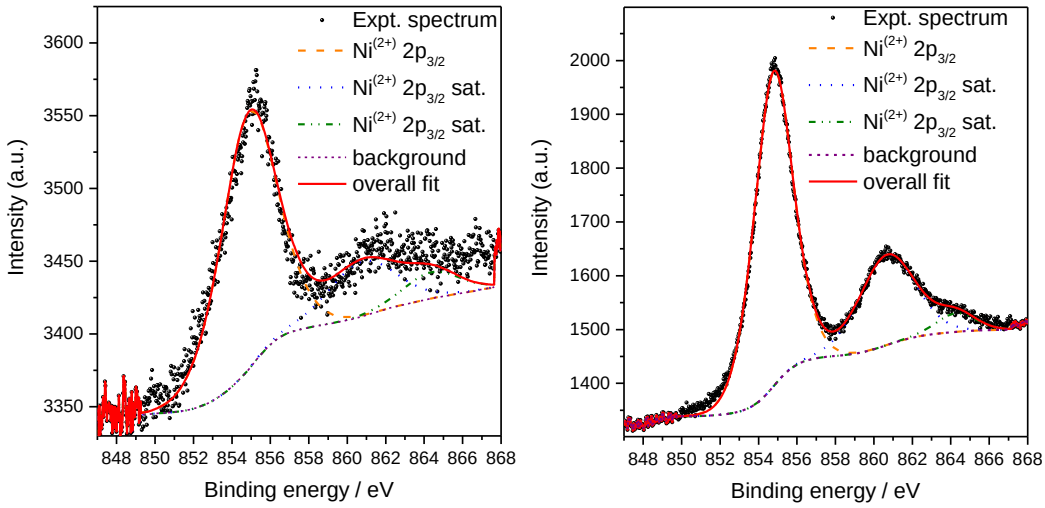

Figure S10 - Experimental and simulated XPS spectra of Ni 2p levels for ZrO2/NiCycP (left) and NiCycP (right)

2.5 Screening of RuP:NiCycP ratios:

Figure S11 shows the CO yield at 7 hours for a series of ZrO_2/RuP/NiCycP catalyst suspensions prepared using an ethanolic solution with the indicated RuP:NiCycP ratio. The surface loadings of RuP and NiCycP were measured by ICP analysis, see section 2.1 above, to give the measured TON. On the basis of this initial study samples using a 5:1 soaking solution were used in all other works.

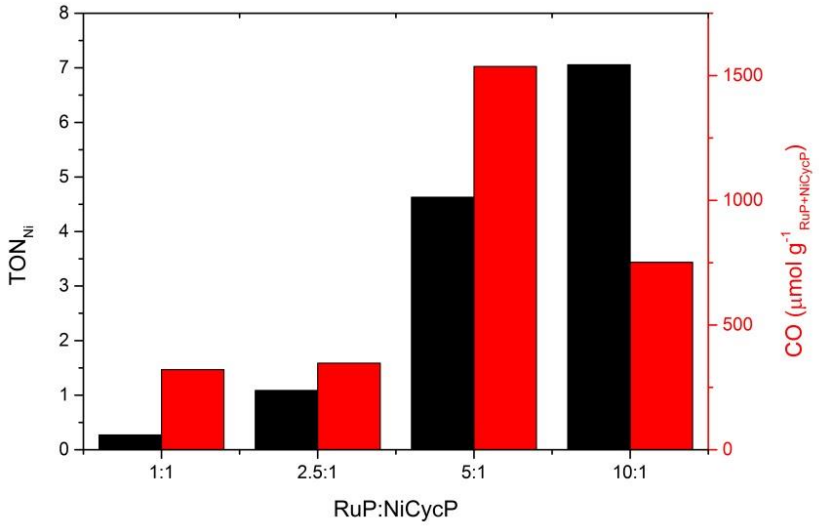

Figure S11 - Photocatalytic CO yield normalised for the combined mass of RuP and NiCycP for a range of RuP and NiCycP ratios. Samples are placed in CO_2 purged 0.1 M ascorbate buffer (pH 4) and illuminated (375-795 nm, 50 mW cm^{-2}) for 7 hours.

2.7 Isotopic labelling experiment:

An experiment using $^{13}CO_2$ was carried out to ensure CO_2 is the carbon source for the CO produced. A sample containing 15 mg of ZrO_2 nanoparticles in 15 ml of ascorbate buffer (0.1 M, pH = 4) was purged for 3 minutes with $^{13}CO_2$ (Sigma) and irradiated for 48 hours under constant stirring. 1.5 ml of the headspace gas was injected into an argon-purged, custom made gas IR cell. The FTIR spectrum primarily (70%) shows ^{13}CO (centred at 2098 cm^{-1}) confirming that the majority of the product originates from the $^{13}CO_2$. It was notable that in this experiment, which required prolonged irradiation (48 hrs) to achieve a sufficient quantity of CO to be readily measurable by our FTIR apparatus, approximately 30% of the total CO in the headspace (determined by subtraction of a pure ^{12}CO spectrum, centred at 2141 cm^{-1}) was ^{12}CO. To explore the source of the ^{12}CO we have also examined the behaviour of ZrO_2/RuP/NiCycP

samples in ascorbate buffer (0.1 M, pH = 4) under an argon atmosphere under prolonged illumination, Figure S13. At early times <10 hrs we observe minimal CO evolution, in-line with the control experiments in the main text which reported no significant CO production in the absence of CO_2 at 7 hours. However at greater than 24 hours we note a rapid rise in the CO level, which accounts for the observed 30% of ^{12}CO in the FTIR experiment after 48 hours of illumination. This is tentatively attributed to be due to ascorbate breakdown pathways which occur under prolonged illumination. Therefore to ensure that the CO yields in the main text correlate solely to photocatalytic CO_2 reduction all data is reported at 7 hours.

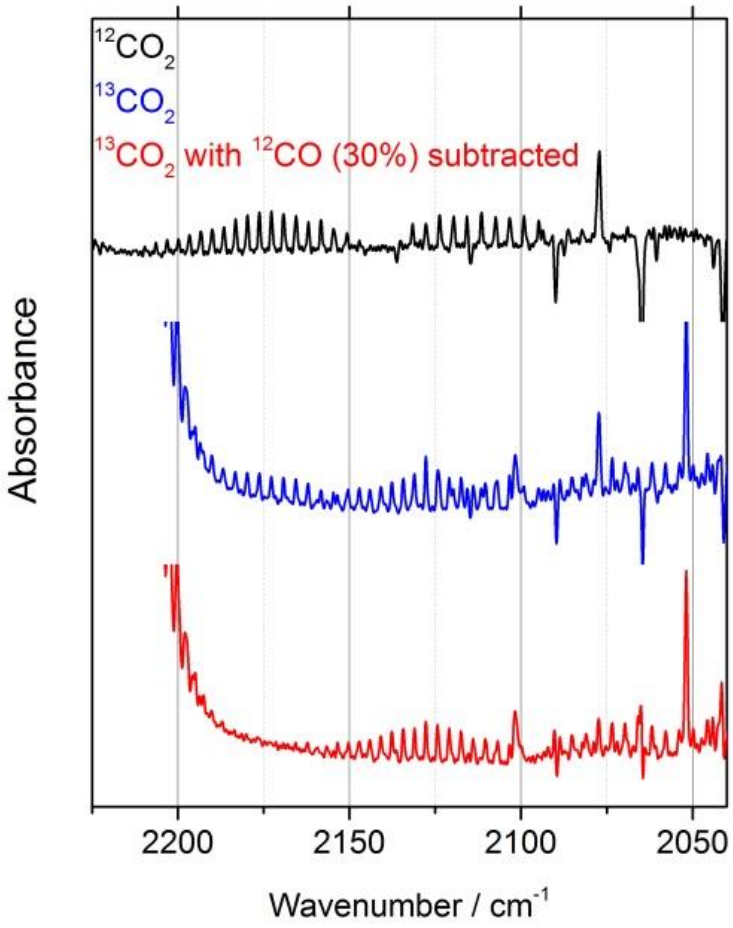

Figure S12 - FTIR spectrum of headspace gases recorded following illumination of ZrO_2/RuP/NiCycP under $^{13}CO_2$ (blue) for 48 hours. The legend refers to the gas used to purge the cell prior to the photocatalysis experiment. The red trace is the FTIR data recorded from the $^{13}CO_2$ experiment with the ^{12}CO manually proportionally subtracted, using this method we calculate ca. 70% ^{13}CO is formed and 30% ^{12}CO is formed.

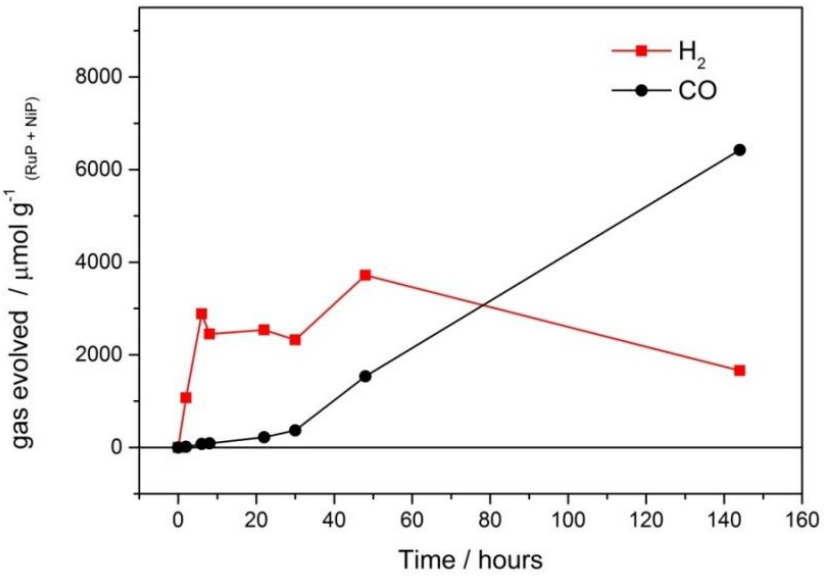

Figure S13 - Photocatalytic CO and H_2 yields normalised for the combined mass of RuP and NiCycP for a ZrO_2/RuP/NiCycP (5:1) sample under Argon irradiated with 375-795 nm light, 50 mW cm^{-2}.

2.8 Visible light photocatalysis

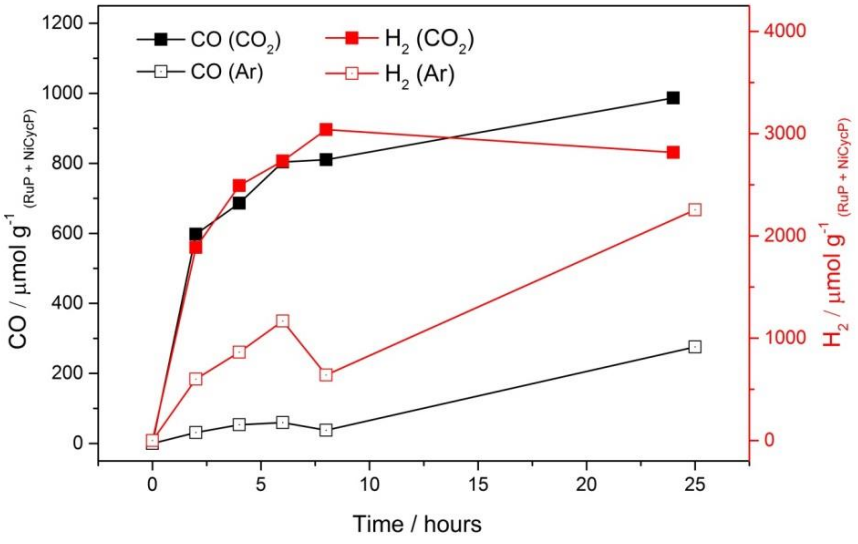

Figure S14 - Photocatalytic CO and H_2 yields normalised for the combined mass of RuP and NiCycP for a ZrO_2/RuP/NiCycP (5:1) sample under Argon (open symbols) and CO_2 (filled symbols) irradiated with 420-795 nm light, 50 mW cm^{-2}.

2.9 Transient spectroscopy

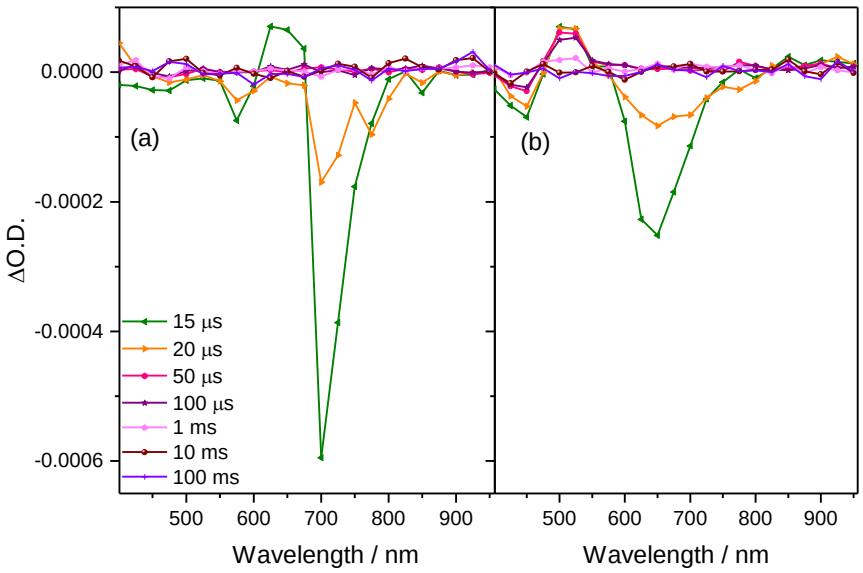

Figure S15 - TA spectra of ZrO_2/Ru P in H_2O (a) and (b) 0.1 M ascorbate (pH 4) following 355 nm (6 ns) excitation at the time delays indicated.

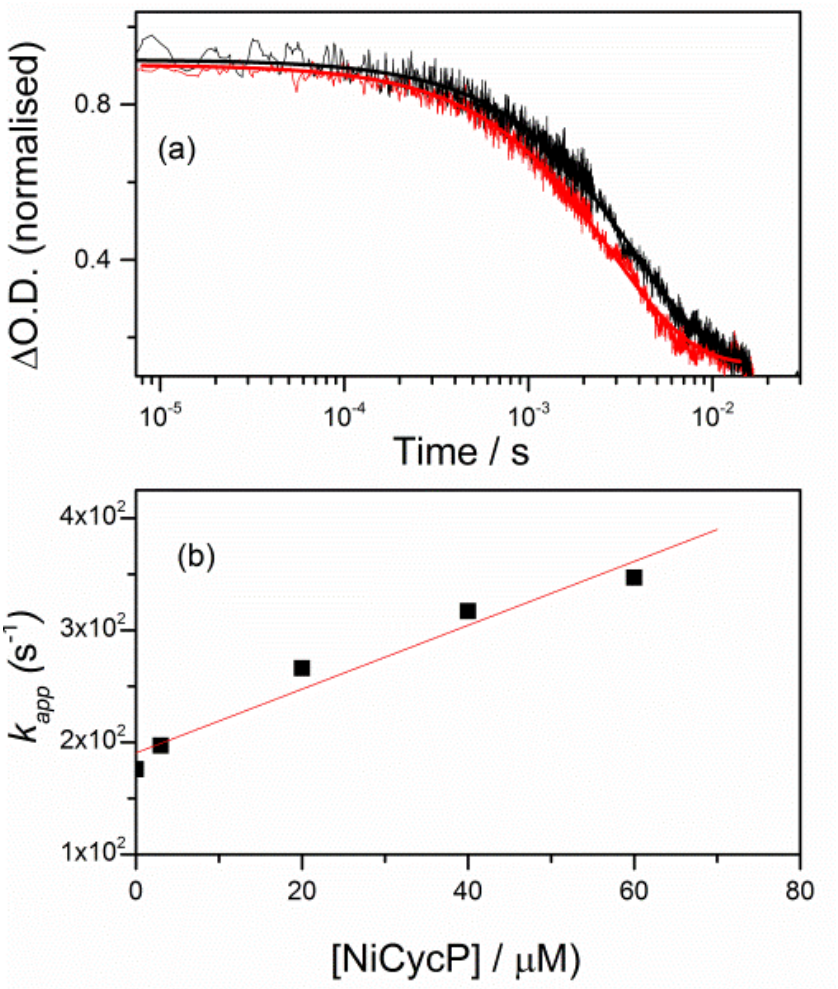

Figure S16 - (a) Kinetic traces recorded at 510 nm of RuP^- in solution formed following 355 nm excitation of RuP (9 μM) in a argon purged 0.1 M ascorbate in the absence (black line) and presence of NiCycP (60 μM, red line). (b) NiCycP concentration dependence for the apparent rate constant of RuP^- loss (k_{app}) in solution.

2.10 Emission spectroscopy

Using time-resolved photoluminescence (TR-PL) it is found that the lifetime of the RuP* state of ZrO_2/RuP is significantly shorter (447 ± 6 ns) than the time-resolution of our TA experiment (*ca.* 2 μs) and only the tail of the RuP* population is observed in Figure S15. In the presence of 0.1 M ascorbate buffer (pH 4) the lifetime of RuP* decreases to 186 ± 5 ns due to reductive quenching of RuP*, in-line with past reports, Fig S17.[9] Steady state emission studies indicate a *ca.* 60% decrease in RuP* emission in the presence of 0.1 M ascorbate buffer, Figure S18.

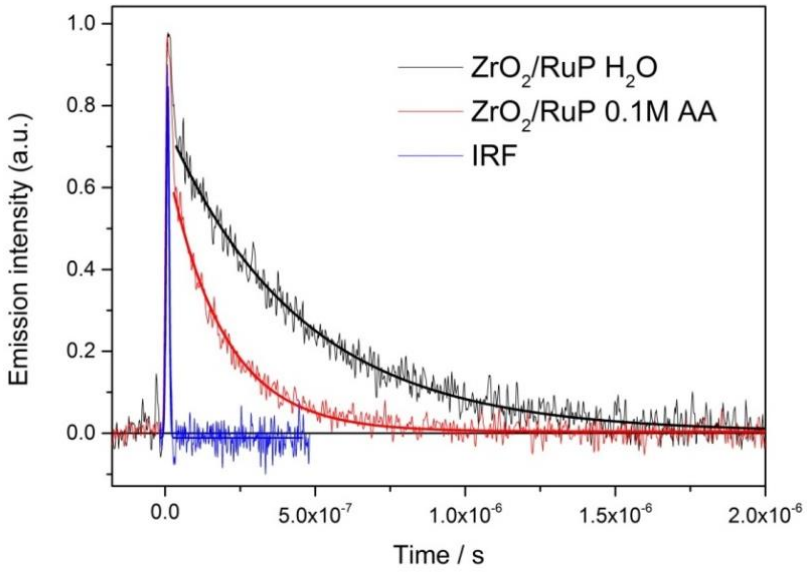

Figure S17 - TR-PL recorded at 650 nm following 355 nm excitation of ZrO_2/RuP in argon purged (black trace) water (pH 4, HCl) and 0.1 M ascorbate buffer (pH 4, red trace). The instrument response function is shown in blue.

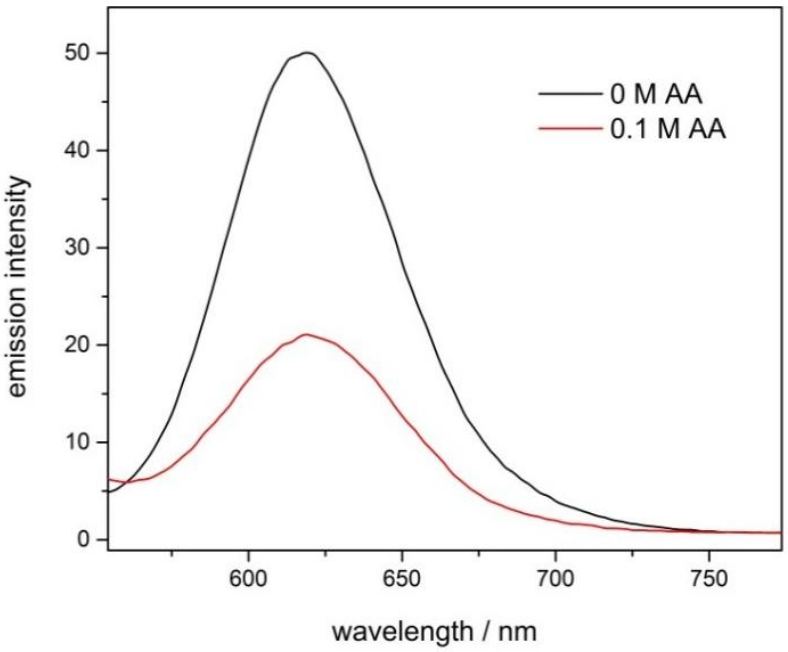

Figure S18 - PL recorded following excitation at 435 nm of ZrO_2/RuP in argon purged (black trace) water (pH 4, HCl) and 0.1 M ascorbate buffer (pH 4, red trace).

2.11 Photocatalytic selectivity

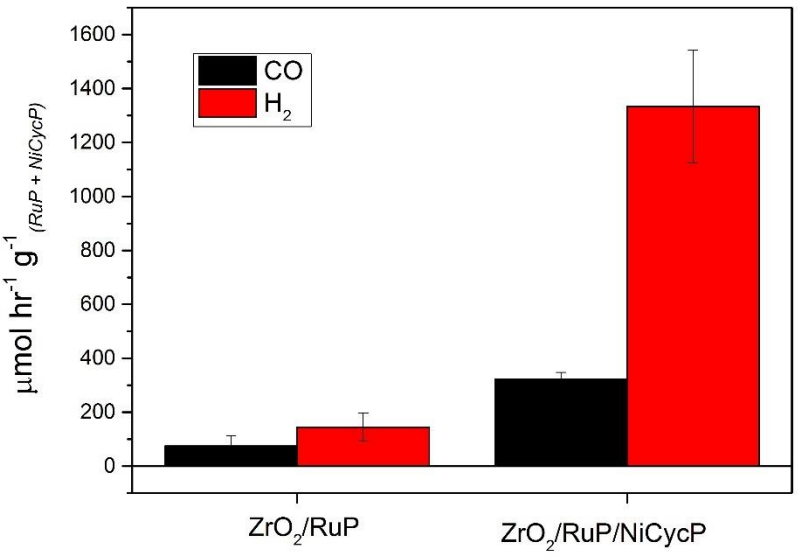

Figure S 19 - Photocatalytic CO and H2 evolution rates for ZrO2/RuP and ZrO2/RuP/NiCycP normalised for the combined mass of RuP and NiCycP. Samples are placed in CO2 purged 0.1 M ascorbate buffer (pH 4) and illuminated (375-795 nm, 40 mW cm-2) for 7 hours.

The selectivity of ZrO_2/RuP/NiCycP for H_2:CO (4.15) is in-line with the past reports of Ru(II) dyes in solution with NiCyc at this pH (see main text). However as NiCyc is known to be a highly selective electrocatalyst in aqueous solutions for CO_2 reduction it is of interest to explore the possible causes for the high level of H_2. One possibility is that RuP in aqueous solution may be either able to directly photocatalytic produce H_2 or a RuP breakdown product may lead to H_2 evolution. Figure S 19 does show that substantial H_2 evolution does occur from ZrO_2/RuP alone, however it is notable that the rate of H_2 formation is still well below that observed for ZrO_2/RuP/NiCycP. Alternative causes of the high level of H_2 evolution could be due to the interaction of oxidised ascorbate breakdown products and future work will explore the role of scavengers in controlling both activity and selectivity towards CO_2.

3. Kinetic analysis of electron transfer to NiCycP:

Our analysis is based on a model developed by Herrero and co-workers[18] for the quenching of a related ruthenium dye by NiCyc in solution, which is briefly outlined below. It is proposed the RuP^-, generated following the excitation of RuP and subsequent reductive quenching by ascorbate (AA), either undergoes electron transfer to NiCycP or is consumed by a competitive back reaction with oxidised ascorbate ($AA^{+\cdot}$), Scheme S1.

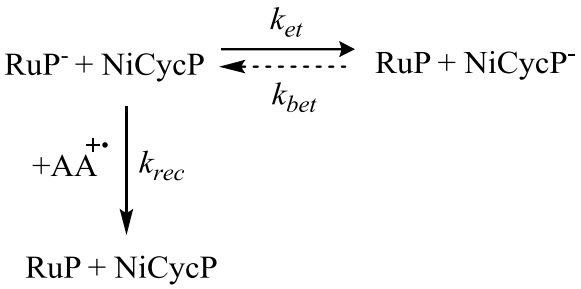

Scheme S1 - Loss pathways for RuP^- formed following the reductive quenching of RuP in 0.1 M ascorbate (pH 4).*

Similar to the previous report[18] we observe pseudo-first order kinetics for the decay of RuP^- proposed to be due to the presence of a significant quantity of oxidised ascorbate even when the highest purity reagents were used. This gives rise to a concentration of oxidised ascorbate species that greatly exceeds that of the photogenerated RuP^- either in solution or on the ZrO_2 surface. In this kinetic analysis we do not consider the rate of back electron transfer between $NiCycP^-$ and RuP as it is shown in the main text that this is likely to be thermodynamically unfavoured by *ca.* +0.3 eV. We also note that the concentration of $Ni^{II}CycP$ is expected to greatly exceed that of RuP^- as: (i) excitation of ZrO_2/RuP/NiCycP at the low laser intensities used here is calculated to lead to a maximum concentration of RuP^- (*ca.* 10^{13} molecules cm^{-2}) per laser pulse that is well below the calculated concentration of NiCycP on the ZrO_2 film (*ca.* 10^{15} molecules cm^{-2}) and (ii) we also use a short laser pulse at very low (0.33 Hz) repetition rate to prevent the build-up of reduced $NiCycP^-$. Therefore in this simplified kinetic scheme we approximate $[NiCycP]_t \sim [NiCycP]_0$. This leads to the following rate equation for the loss of RuP^-:

$$\frac{d[RuP^-]}{dt} = -k_{et}[RuP^-][NiCycP]_0 - k_{rec}[RuP^-][AA^{+\cdot}]_0$$

$$\frac{d[RuP^-]}{dt} = -k_{app}[RuP^-]$$

$$k_{app} = k_{rec}[AA^{+\cdot}]_0 + k_{et}[NiCycP]_0$$

The rate of decay of RuP^- was monitored at 510 nm using transient spectroscopy and fitted to either a monoexponential decay (for solution experiments) or to a stretched monoexponential decay (for ZrO_2/RuP and ZrO_2/RuP/NiCycP) of the form $\Delta OD_{510\ nm} = y_0 + A_1 e^{-(kt)^{\beta}}$, β = 0.65 reflecting the variety of potential surface sites on commercial ZrO_2 nanoparticles, giving rise to the apparent rate constant k_{app}.

For ZrO_2/RuP films we measure k_{app} = 1.4 x 10^3 $s^{-1} \approx k_{rec}[AA^{+\cdot}]_0$. The presence of NiCycP on ZrO_2/RuP/NiCycP increases k_{app} = 7.8 x 10^3 s^{-1}. Assuming that k_{rec} is independent of the presence of NiCycP this gives an estimated $k_{et}[NiCycP]_0$ = 6.4 x 10^3 s^{-1} and an approximate relative electron transfer yield of 82%.

$$\Phi_{NiCycP^-} = \frac{k_{et}[NiCycP]_0}{k_{et}[NiCycP]_0 + k_{rec}[AA^{+\cdot}]_0}$$

Using the concentrations of RuP and NiCycP employed in the solution photocatalysis studies (these employ an equivalent quantity of NiCycP and RuP within the 2 ml of solution as are present in the 2 ml ZrO_2/RuP/NiCycP suspension experiment) we measure $k_{app} \approx$ 1.9 x 10^2 s^{-1}. In the absence of NiCycP $k_{app} \approx$ 1.8 x 10^2 $s^{-1} \approx k_{rec}[AA^{+\cdot}]_0$. This leads to an estimated solution $k_{et}[NiCycP]_0$ = 0.1 x 10^2 s^{-1} and an associated electron transfer yield of only 5%. We recognise the inaccuracies relating to deriving such a number from a single concentration of NiCycP therefore in solution we have also measured the variation of k_{app} at a wider range of NiCycP concentrations and from the slope of Fig S16 we obtain k_{et} = 2.8 x 10^6 M^{-1} s^{-1}, which is in reasonable agreement with the single point measurement from which the electron transfer yield is derived.

4. Calculated surface coverages:

The commercial supplier of the ZrO_2 nanoparticles states the upper limit of the particles as being ~100 nm.

The surface area of one particle is:

$$4\pi(50\text{x}10^{-9})^2 = 3.14\text{x}10^{-14}\text{m}^2 \text{ or } 3.14\text{x}10^{-10}\text{cm}^2$$

With a volume of:

$$4\pi(\frac{50\text{x}10^{-9})^3}{3}) = 5.24\text{x}10^{-22}\text{m}^3 \text{ or } 5.24\text{x}10^{-16}\text{cm}^3$$

In an ICP experiment 5 mg of ZrO_2 is used, d = 5.89 g cm^{-3}, therefore the number of ZrO_2 nanoparticles in an ICP study:

$$\frac{\left(\frac{5\text{x}10^{-3}}{5.89}\right)}{5.24\text{x}10^{-16}} = 1.62\text{x}10^{12} \text{ particles}$$

With a combined surface area of:

$$(1.62 \text{ x } 10^{12}) \text{ x } (3.14 \text{ x } 10^{-10}) = 508 \text{ cm}^2$$

In the initial study of catalyst loadings (Figure S11) from the 5:1 RuP to NiCycP experiments the ICP measured Ru and Ni concentrations in the NaOH stripping solution (5 ml) were 0.900 mg dm^{-3} (Ru) and 0.197 mg dm^{-3} (Ni) (Table S1). This corresponds to $4.5\text{x}10^{-8}$ and $1.7\text{x}10^{-8}$ moles of RuP and NiCycP from 5 mg ZrO_2. The number concentration of NiCyP per ZrO_2 particle is:

$(1.7\text{x}10^{-8} \text{ x } N_A)/1.62\text{x}10^{12} = 6.3 \text{ x}10^3$ molecules per ZrO_2 particle

The number concentration of RuP per ZrO_2 particle is:

$(4.5\text{x}10^{-8} \text{ x } N_A)/1.62\text{x}10^{12} = 1.7 \text{ x}10^4$ molecules per ZrO_2 particle

Based on crystal structure data we estimate a footprint of $8 \text{ x}10^{-15}$ cm^2 for NiCycP and $1.65 \text{ x}10^{-14}$ cm^2 for RuP. This leads to an estimated coverage of:

NiCycP = $(8 \text{ x}10^{-15} \text{ x } 6.3\text{x}10^3)/3.14\text{x}10^{-10} = 0.16$ or 16% (correlating to 0.2 NiCycP nm^{-2})

RuP = $(1.65 \text{ x}10^{-14} \text{ x } 1.7\text{x}10^4)/3.14\text{x}10^{-10} = 0.89$ or 89% (correlating to 0.5 RuP nm^{-2})

The overall estimated coverage is slightly greater than 1 monolayer (105%), however it should be noted that significant uncertainties are present in the calculation above, in particular the structure of NiCycP and hence its foot-print when immobilised is unknown. Therefore the values should be used with caution.

5. References:

1. F. Lakadamyali, A. Reynal, M. Kato, J. R. Durrant, and E. Reisner, *Chem. Eur. J.*, 2012, **18**, 15464–15475.
2. I. Gillaizeau-Gauthier, F. Odobel, M. Alebbi, R. Argazzi, E. Costa, C. A. Bignozzi, P. Qu, and G. J. Meyer, *Inorg. Chem.*, 2001, **40**, 6073–6079.
3. S. Füzerová, J. Kotek, I. Císařová, P. Hermann, K. Binnemans, and I. Lukeš, *Dalt. Trans.*, 2005, 2908–2915.
4. Bruker, *APEX II*, 2009, Bruker AXS Inc., Madison, Wisconsin, USA.

5. O. V. Dolomanov, L. J. Bourhis, R. J. Gildea, J. A. K. Howard, and H. Puschmann, *J. Appl. Crystallogr.*, 2009, **42**, 339–341.

6. G. M. Sheldrick, *Acta Crystallogr. A*, 2007, 64, 112–122.

7. M. Forster, R. J. Potter, Y. Ling, Y. Yang, D. R. Klug, Y. Li, and A. J. Cowan, *Chem. Sci.*, 2015, **6**, 4009–4016.

8. B. Bosnich, M. L. Tobe, and G. A. Webb, *Inorg. Chem.*, 1965, **4**, 1109–1112.

9. M. A. Gross, A. Reynal, J. R. Durrant, and E. Reisner, *J. Am. Chem. Soc.*, 2014, **136**, 356–366.

10. M. C. Zenobi, C. V. Luengo, M. J. Avena, and E. H. Rueda, *Spectrochim. Acta - Part A Mol. Biomol. Spectrosc.*, 2008, **70**, 270–276.

11. A. G. Menke and F. Walmsley, *Inorganica Chim. Acta*, 1976, **17**, 193–197.

12. W. C. Grinonneau, P. L. Chapman, A. G. Menke, and F. Walmsley, *J. Inorg. Nucl. Chem.*, 1971, **33**, 3011–3017.

13. D. J. Morgan, *Surf. Interface Anal.*, 2015, **47**, 1072–1079.

14. B. Varughese, S. Chellamma, and M. Lieberman, *Langmuir*, 2002, **18**, 7964–7970.

15. Y. Zhang, C. Bao, G. Wang, Y. Song, L. Jiang, Y. Song, K. Wang, and D. Zhu, *Surf. Interface Anal.*, 2006, **38**, 1372–1376.

16. B. P. Payne, A. P. Grosvenor, M. C. Biesinger, B. A. Kobe, and N. S. McIntyre, *Surf. Interface Anal.*, 2007, **39**, 582–592.

17. L. M. Moroney, R. S. C. Smart, and M. W. Roberts, *J. Chem. Soc. Faraday Trans. 1 Phys. Chem. Condens. Phases*, 1983, **79**, 1769.

18. C. Herrero, A. Quaranta, S. El Ghachtouli, B. Vauzeilles, W. Leibl, and A. Aukauloo, *Phys. Chem. Chem. Phys.*, 2014, **16**, 12067.